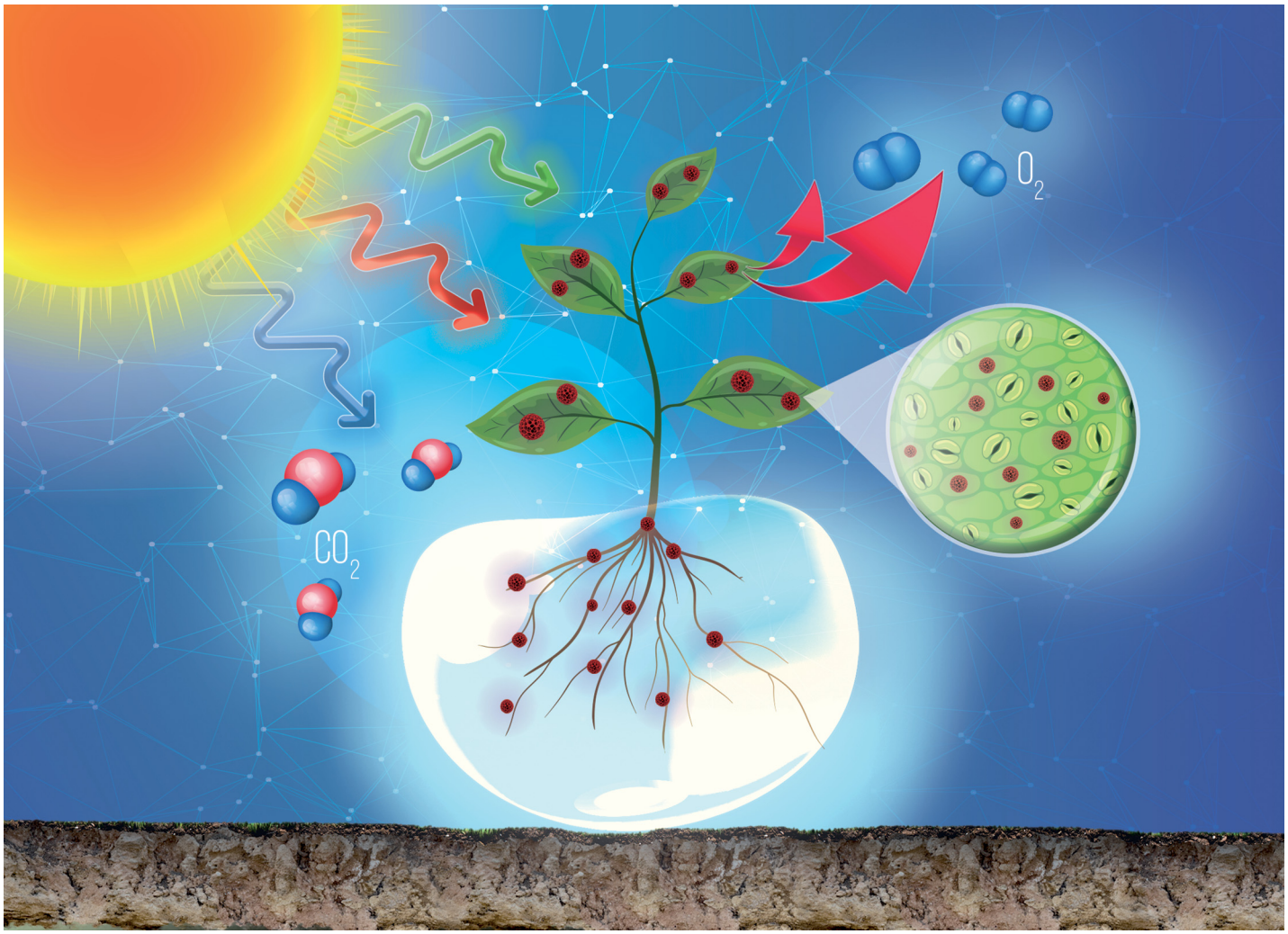

Highlighting research from the Free University of Bozen-Bolzano, Faculty of Engineering.

Conjugated polymer nanoparticles boosting growth and photosynthesis in biohybrid plants

This work reports the first *in vivo* integration of poly(3-hexylthiophene) nanoparticles (P3HT-NPs) into *Arabidopsis thaliana* plants, creating a bio-hybrid plant with enhanced growth and photosynthetic performance. Through morphological, optical, and chemical characterization, we demonstrate that P3HT-NPs act as photonic antennas, broadening light absorption and facilitating electron transfer within the photosynthetic machinery. The study opens new perspectives for sustainable bio-nanotechnology approaches to improve plant productivity and renewable energy harvesting.

Image reproduced by permission of Manuela Ciocca from *Mater. Horiz.*, 2025, **12**, 7937.

As featured in:

See Manuela Ciocca *et al.*, *Mater. Horiz.*, 2025, **12**, 7937.

ROYAL SOCIETY OF CHEMISTRY

rsc.li/materials-horizons

Registered charity number: 207890

Materials Horizons

ROYAL SOCIETY OF CHEMISTRY

COMMUNICATION

View Article Online
View Journal | View Issue

Cite this: *Mater. Horiz.*, 2025, **12**, 7937

Received 25th February 2025,
Accepted 25th July 2025

DOI: 10.1039/d5mh00341e

rsc.li/materials-horizons

Conjugated polymer nanoparticles boosting growth and photosynthesis in biohybrid plants

Manuela Ciocca,*[a] Mauro Maver,[b] Ciro Allará,[a] Damiano Zanotelli,[c] Soufiane Krik,[a] Antonio Orlando,[ad] Thilo Rühle,[e] Sabrina Walz,[e] Theo Figueroa Gonzalez,[e] Giovanna Gentile,[af] Alexandros A. Lavdas,[f] Pietro Ibba,[a] Fabio Trevisan,†[b] Zygmunt Milosz,[g] Melanie Timpel,[h] Marco V. Nardi,[h] Andrea Pedrielli,[d] Andrea Gaiardo,[d] Paolo Lugli,[a] Franco Cacialli,[a] Dario Leister,[e] Tanja Mimmo[bc] and Luisa Petti[ab]

Engineered nanomaterials integrated into photosynthetic systems could pave the way to new, exciting avenues towards biohybrid systems and renewable energy sources. Here, a biohybrid plant developed through the integration of poly(3-hexylthiophene) nanoparticles (P3HT-NPs) in *Arabidopsis thaliana* plants is presented. P3HT-NPs were used to enhance plant solar radiation absorption, with a spectrophotometric profile matching chlorophyll absorbance. The P3HT-NP-engineered biohybrid plants showed a 45% increase in root length, corresponding to a relevant enhancement in biomass production of up to 17% compared to the control group. The presented biohybrid plant might open a new route for improving CO_2 capture and oxygen production, underscoring the transformative potential of combining nanomaterials with plant biology, and paving the way for novel biohybrid nano-engineered renewable energy sources.

New concepts

This work demonstrates a novel concept in materials science: the *in vivo* integration of conjugated polymer nanoparticles (CP-NPs), namely poly(3-hexylthiophene) nanoparticles (P3HT-NPs) into *Arabidopsis thaliana* plants, to form a bio-hybrid photosynthetic living system. The presented first engineered bio-hybrid plant shows enhanced photosynthetic efficiency and growth. Unlike previous studies that have focused on *ex vivo* applications or toxicity assessments of nanomaterials in plants, our approach directly incorporates P3HT-NPs into the plant's 3D structure. The P3HT-NPs act as photonic antennas, potentially interacting with native chlorophyll to broaden light absorption and boost electron transfer during photosynthesis. As a result, treated plants exhibit an 11% increase in CO_2 assimilation and significant improvements in biomass accumulation, up to 17%. This work provides new insights into how engineered nanomaterials can be harnessed to modify intrinsic biological energy conversion processes, thereby bridging the fields of nanomaterials and plant biology. The concept not only advances our understanding of nano–bio interactions but also opens promising avenues for novel sustainable bio-hybrid nano-engineered energy sources.

Introduction

Photosynthetic systems (*e.g.*, plants, algae, and bacteria) are vital for energy harvesting in nearly all Earth ecosystems. They transform carbon dioxide (CO_2, from the atmosphere) and water (H_2O, from soil) into carbohydrates, and release oxygen into the atmosphere by utilizing electromagnetic energy, typically from the sun,[1] through the natural photosynthesis process. In plants, this primarily takes place in the leaves, and more specifically within the chloroplasts (specialised plant cell organelles) where light reactions occur in sac-like structures known as thylakoids. Light is captured mainly by the green dyes of chlorophyll (located in the thylakoid membrane).[2] The structure of chlorophyll shows a five-ring heterocyclic structure surrounding Mg^{2+} ions with an extended (conjugated) polyene moiety alternating single and double bonds, responsible for absorption in the visible region of the electromagnetic spectrum (Fig. S1a). Thus, as a principal photoreceptor, chlorophyll harvests the absorbed solar energy and makes it available for several chemical reactions whose final product is sugar,[3] consistently with the following eqn (I) and (II):[4]

$$2H_2O \xrightarrow{\text{Light}} O_2 + 4[H^+] + 4e^- \quad \text{(I)}$$

$$4e^- + 4[H^+] + CO_2 \rightarrow (CH_2O) + H_2O \quad \text{(II)}$$

[a] *Faculty of Engineering, Free University of Bozen-Bolzano, via Bruno Buozzi 1, 39100 Bolzano, Italy. E-mail: manuela.ciocca@unibz.it*
[b] *Competence Centre for Plant Health, Free University of Bozen-Bolzano, Piazza Università 5, 39100 Bolzano, Italy*
[c] *Faculty of Agricultural, Environmental and Food Sciences, Free University of Bozen-Bolzano, Piazza Università 5, 39100 Bolzano, Italy*
[d] *Sensors and Devices Center, Bruno Kessler Foundation, via Sommarive, 18, I-38123 Povo (TN), Italy*
[e] *Plant Molecular Biology, Faculty of Biology, Ludwig-Maximilians-University Munich, D-82152 Planegg-Martinsried, Germany*
[f] *Institute for Biomedicine, Eurac Research, via A. Volta 21, 39100 Bolzano, Italy*
[g] *Elettra – Sincrotrone Trieste S.C.p.A, Strada Statale 14 – km 163,5 in AREA Science Park, 34149, Trieste, Italy*
[h] *IMEM-CNR Institute of Materials for Electronics and Magnetism, Trento Unit C/o Fondazione Bruno Kessler, Via Alla Cascata 56/C, Povo, 38123, Trento, Italy*
† This author is deceased.

Radiation with wavelength in the range of 400 to 700 nm, known as photosynthetically active radiation (PAR), is universally used as a source of energy for photosynthesis by green plants.[5] The main forms of chlorophyll in plants are chlorophyll *a* (Chl *a*, absorption peaks at 430 and 663 nm) and chlorophyll *b* (Chl *b*, absorption peaks at 450 and 640 nm) generally in a ratio of 3 : 1[6,7] (Fig. S1a). Thus, by absorbing maximally in the blue (430–450 nm) and red (640–663 nm) regions of the solar spectrum, chlorophyll–protein complexes are involved in harvesting solar energy and transporting electrons, resulting in the generation of the reductant (such as nicotinamide adenine dinucleotide phosphate (NADPH), which carries electrons for the next steps of the photosynthetic process) and energy (adenosine triphosphate (ATP), which serves as an energy currency in the cell).[8]

Plants convert, utilize, and store less than 1% of the solar energy.[9] Solar energy is the most environmentally friendly and sustainable energy source. In the last few decades, solar-driven CO_2 conversion applied to the production of fuels has received increasing attention within a vision of a future based on renewable energy sources.[10] From this perspective, photocatalytic, photoelectrochemical, and photovoltaic (PV) plus electrochemical approaches have been intensively studied strategies.[10] The emerging and fast-expanding research field of engineered and hybrid living materials (ELMs and HLMs) that combine living and non-living matter is currently establishing a promising perspective for achieving such an aim,[11–13] offering unprecedented opportunities to develop novel and non-genetic strategies for sustainably enhancing the efficiency of photosynthetic systems,[14] moving beyond the limitations of traditional genetic engineering approaches. Developing HLMs for energy production could potentially overcome a variety of conventional approaches (*e.g.*, PV) to these issues. So far, however, only simple biological model systems (*e.g.*, bacteria and microalgae) have been used for the realization of energy conversion-HLMs,[15–17] whereas plants remain still mostly unexplored as testbeds for the development of biohybrid living systems. Only very recently, organic PV polymers and nanomaterials have been introduced in plant biotechnologies, with the aim of both enhancing photosynthesis and monitoring plant functions.[18,19] Although knowledge of the interactions of nanoparticles (*e.g.*, gold, carbon) with plants has increased,[20–25] the development of biohybrid plants *via* interfacing them with engineered nanoparticles (NPs) for controlled energy conversion is still a distant prospect. Carbon dots (CDs), with absorption capability across the UV and visible range and emission into far-red/near-infrared (NIR) light (625 to 800 nm), have been explored for artificial photosynthesis to extend the plants' solar light utilization.[26] Despite the promising enhancement of the photosynthesis, enabled by the far-red/NIR emitting CDs, demonstrated *in vitro*, the long-term biocompatibility in diverse plant systems, and the limited understanding of CD interactions with plant cellular pathways are still unresolved challenges. While successful *in vivo* incorporation of CDs as light-harvesting antennas has been demonstrated in unicellular cyanobacteria (*Synechococcus elongatus*), achieving such an aim in plant leaves remains under investigation.[27] Recent efforts have been focused on using CDs and doped-CDs to create chloroplast-hybrid systems to enhance chlorophyll light absorption and improve photosynthesis.[26,28,29] A major limitation of these studies lies in the fact that the enhancement of photosynthetic performance was demonstrated through direct measurements only in isolated chloroplast systems, while *in planta* investigations relied on indirect indicators such as leaf fluorescence, biomass accumulation, and morphological traits.

Other engineered biosafe nanomaterials, with photoconversion properties can be considered for this purpose. For instance, conjugated polymers (CPs) are outstanding light-harvesting materials with large absorption coefficients,[30] demonstrating biocompatibility[31,32] and high tunability of their optical properties.[33,34] They are widely used in organic PVs[35] as thin films or as nanostructures (in the form of nanofibers or NPs).[36] Lately, the use of CP thin films and CP-NPs has been proposed for application in the general area of bioelectronics, biophotonics and photovoltaic bioelectronics[37,38] to monitor and stimulate bioelectrical activity of living cells.[39,40] Recently CPs were employed to indirectly enhance photosynthesis by interfacing CP-NPs with chloroplasts[41] or plant leaves affecting the *Arabidopsis thaliana* (*A. thaliana*) stomatal aperture (leaf pores regulating transpiration) and indirectly influencing the photosynthesis.[18] CP-NPs were also proposed as artificial antennas to expand the PAR range of natural pigments for application in artificial photosynthesis[42] and artificial carbon sequestration.[43] An *in vitro* model of chitosan-modified CP-NPs was investigated to increase photosynthetic efficiency and plant CO_2 storage.[19] Recently, a blend consisting of poly(3,4-ethylene dioxythiophene) doped with poly(styrene sulfonate) (PEDOT:PSS) and carboxymethylated cellulose nanofibrils was exploited to develop the ''eSoil'', a bioelectronic hydroponic medium providing electrical stimuli on roots of plants and promoting root and shoot growth.[44]

However, the potential of CP-NPs to enhance plant growth and biomass production for engineered bioenergy alternatives has been minimally explored, and there is a lack of direct *in vivo* studies on the existing biohybrid interfaces to gain fully functional enhanced biohybrid photosynthetic systems.

Here, we present the first engineered biohybrid plant through the *in vivo* integration of poly(3-hexylthiophene) nanoparticles (P3HT-NPs) into *A. thaliana* plant model. The unprecedented biohybrid photosynthetic system demonstrates enhanced growth and biomass production, representing a significant step forward at the intersection of nanomaterials and plant biology. The presented approach enables the direct and functional integration of CP-NPs within the three-dimensional architecture of the entire living plant, validating the biosafety of CP-NPs in whole organisms and paving the way for novel biohybrid nano-engineered renewable energy sources.

Experimental

Preparation of P3HT-NPs dispersion

P3HT-NPs dispersion was prepared by the nanoprecipitation method working in a laminar flow hood. Regioregular poly(3-hexylthiophene-2,5-diyl) (rr-P3HT, Mw 60 150, Rr 97.6%, Ossila)

was dissolved in tetrahydrofuran (THF, Merck) at a concentration of 10 mg mL^{-1}. 1 mL of the obtained P3HT solution was added dropwise in 20 mL of ultrapure water (presterilized in an autoclave at 80 °C) under stirring. Thus, P3HT was first dissolved in THF (a good solvent) miscible with water and then dispersed into H_2O (a poor solvent) under stirring. Therefore, NPs were instantaneously formed because of the rapid change in solvent polarity. Thus, a colloidal suspension of P3HT-NPs is obtained. The residual organic solvent, potentially harmful for biological systems, was then removed by dialyzing the colloidal suspension using a dialysis sack (pore size 14 000 MWCO, 99.99% retention) against 2 L of sterilized deionized water overnight. The whole process was carried out in sterile conditions. The obtained P3HT-NPs dispersion was additionally sterilized *via* an autoclave before being mixed in a sterile plant agarose-based hydrogel growth medium and all subsequent steps were carried out under sterile conditions to avoid possible contamination of the biological samples.

P3HT-NPs characterization

P3HT-NPs absorbance and emission spectra were recorded *via* a spectrophotometer (Jasco Corporation V-670) and a fluorimeter (Horiba Fluoromax 4) respectively. For the emission spectra, an excitation wavelength of λ = 500 nm was used.

Nanoparticle size (hydrodynamic diameter) and charge (zeta potential) were measured *via* dynamic light scattering (DLS) with a wavelength of 633 nm in back-scattering mode *via* using a zetasizer ZEN3600 (Malvern Panalytical).

The morphology of the P3HT-NPs was investigated using a scanning and plasma electron microscope – Dual Beam CXe Helios 5 PFIB, from ThermoFisher (Thermo Fisher Scientific, Waltham, Massachusetts, US). The system is equipped with a suite of state-of-art that enable high-resolution S/TEM analysis, energy dispersive X-ray spectrometry (EDXS) microanalysis for compositional measurements, and an electron backscatter diffraction (EBSD) detector for crystallographic analysis. P3HT-NPs solution was drop cast on a silicon substrate and dried at 60 °C before image acquisition.

For chemical and electronic characterization, P3HT-NPs samples (after dialysis and sterilization) were prepared by repeated drop-casting from an aqueous solution (concentration: 0.10 mg mL^{-1}) onto Si wafers with native SiO_2, ensuring sufficient surface coverage. The samples were dried by heating at 60 °C on a hot plate (~20 minutes) and transferred to the ultrahigh vacuum (UHV) analysis chamber.

Scanning photoelectron microscopy (SPEM) characterization was carried out at the ESCA Microscopy beamline of the ELETTRA synchrotron facility in Trieste (Italy) (**https://www.elettra.eu/elettra-beamlines/escamicroscopy.html**) to investigate the surface chemical states of the P3HT-NPs. A soft X-ray photon beam with an energy of 500 eV was focused on a ~150 nm diameter spot on the sample surface. The drop-cast sample was scanned in front of the beam with a positional accuracy of 10 nm. For XPS imaging and spectroscopy, a 100 mm hemispherical electron energy analyzer equipped with a 48-channel detector and an energy resolution better than 200 meV was used. XPS spectra and image data were analyzed using IGOR Pro v9 software.

Ultraviolet photoelectron spectroscopy (UPS) measurements were performed in an UHV analysis chamber equipped with a He-discharge lamp operating at the He I emission line (21.22 eV) and a VSW HA100 hemispherical electron energy analyzer (featuring a PSP power supply and electronic control). The system provides an energy resolution of 0.1 eV for UPS. During the measurements, the sample was biased at −7.1 V.

Seedling and plant growth medium preparation

Arabidopsis thaliana (*A. thaliana*) Col-0 seeds were provided by the Competence Centre for Plant Health of the Free University of Bozen-Bolzano. The seeds were sterilized in 3 steps: (i) washing the seeds with a solution of 70% ethanol (PanReac – AppliChem) + 0.1% SDS (sodium dodecyl sulfate, Merck) in which the seeds were kept for about 1 minute; (ii) washing the seeds with a 70% ethanol solution; (iii) drying the seeds under a laminar flow hood for about 2–3 hours after the removal of excess ethanol from the washing previous steps. At this point the seeds were sown in Petri dishes (120 × 120 × 17 mm) containing a volume of 50 mL of 1/2 Murashige and Skoog salt (MS, Duchefa Biochemie) medium prepared with 0.8% agarose and 0.3% sucrose (MS agarose-based hydrogel (CTRL)) and mixed with silica NPs (Si-NPs, Merck) or P3HT-NPs at different concentrations, all maintained at pH 5.5 with the MES buffer. The medium was previously prepared and subsequently sterilized in an autoclave. After sowing the *A. thaliana* seeds, the plates were closed and sealed and placed for stratification at 4 °C for 72 hours to ensure seed stabilization and to induce synchronous germination in seeds. After stratification, the plates were incubated in growth chambers (GroBanks CLF Plants Climatics) at 22 °C and a day/night cycle of 16/8 hours respectively with 103 μmol m^{-2} s^{-1} of PAR light radiation conditions during day hours, or 12 hours day (full-spectrum white light) and 4 hours green light/8 hours darkness, 5 plates for each condition were prepared, each containing 10 seeds.

Chlorophyll extraction from *Arabidopsis thaliana* leaves

A. thaliana leaves, from the control group, were harvested on the last day of the observation period (T_{end}, 9 days post-germination) and the fresh weight (28.23 ± 4.01 mg) was recorded. Subsequently the leaves were soaked into 4 mL of ethanol (Merck) and left on stirring for 2 hours. The mixture was transferred to a mortar and pestle and ground for a few minutes. Then, it was filtered. The filtered solution was used for further investigations.

MS and MS + P3HT agarose-based hydrogel medium characterization

PH measurements. pH measurements were conducted at RT using the sensION TM + PH 3 pH meter to assess the pH levels of the agarose-based hydrogel medium before seedling and at the end of the experimental observation period. To facilitate the measurements, a 3 mL volume of agarose-based hydrogel medium was dissolved through heating at 80 °C on a hot plate

for 30 minutes with continuous stirring and subsequently positioned on the pH-meter stage for analysis.

H_2O_2 analysis. Colorimetric analyses were conducted using the MQuant® Peroxide test kit (Merck). Briefly, the peroxidase enzyme is responsible for transferring peroxide oxygen to an organic redox indicator. As a result, a blue oxidation product is produced. Thus, the peroxide test strips go through a blue colour change based on the quantity of H_2O_2 formed in the agarose-based hydrogel soil providing a semi-quantitative measurement of the peroxide concentration *via* visually comparing the test strip's reaction zone with a provided colorimetric scale. In our approach, MATLAB was employed to upload images of the strips, reproduce the colorimetric scale, and statistically compare the images. Following image preprocessing, which involved loading and normalizing the scale and strip images, the mean of the matrices was computed for both. Subsequently, the mean scale matrices were plotted as coloured strips along the *x*-axis, representing the colour spectrum, while the mean strip matrices were plotted as symbols along the *y*-axis. Strips falling within a particular colour band on the scale were associated with that colour. This method allowed for a quantitative analysis of the colorimetric data, enhancing the accuracy and efficiency of our assessment.

Absorbance spectra. Absorbance spectra of extracted chlorophyll from *A. thaliana* leaves, of MS agarose-based hydrogel medium and MS medium supplemented with Si-NPs and P3HT-NPs were acquired through UV-Vis spectrophotometer (Cary 60 UV-Vis, Agilent Technologies). To facilitate the measurements, a 3 mL volume of agarose-based hydrogel medium (supplemented or not with NPs) was dissolved through heating at 80 °C on a hot plate for 30 minutes with continuous stirring and subsequently analysed through the UV-Vis absorbance spectra measurements. Data were analysed *via* OriginPro 2021.

Arabidopsis thaliana roots length and leaves area

A. thaliana root length and leaf area analysis was conducted using ImageJ's image processing software (version 1.54i, National Institutes of Health, Bethesda, MD, USA). Plant samples were imaged using a digital camera with a standard resolution of 50 megapixels and uniform illumination to minimize variations in brightness between images. Following image acquisition, the acquired images underwent preliminary processing to enhance quality and reduce noise, including colour balance adjustment, illumination correction, and removal of any undesired artefacts. Subsequently roots and leaf areas were extracted from the acquired images. The dimensions of the regions of interest (ROIs) corresponding to the roots and leaves were then measured in terms of linear and square pixels respectively using ImageJ. Calibration to convert dimensions into physical units (linear and square centimetres) was done using a reference image with known scales. Data were analysed *via* OriginPro 2021. Statistical analysis was performed *via* one-way ANOVA tests (Tukey test) to evaluate significant differences ($*p < 0.05$, $**p < 0.01$, $***p < 0.001$) in leaf area dimensions and root length among different experimental conditions.

Arabidopsis thaliana fresh and dry weight

Fresh and dry weights of *A. thaliana* were measured by carefully excising plants at the junction between the stem and roots and subsequently placing the roots and stems separately into pre-weighed Eppendorf tubes. After weighing the Eppendorf tubes containing the biomass, they were placed in an oven and left at 60 °C overnight to ensure thorough drying. Following this drying period, the Eppendorf tubes were reweighed to determine the dry weights of the plant material.

Photosynthetic activity measurements

The photosynthetic activity was assessed measuring the net CO_2 exchange of all the plates using an infrared gas analyser (LI-8100, LI-COR Biosciences, Lincoln, NE, USA) adapted to sample the gas from a custom-made Plexiglass chamber fabricated *via* laser cutting, with internal dimensions of 125 × 125 × 27 mm, where each plate was inserted (Fig. S11a). A comprehensive leak test was performed to ensure the reliability of the enclosure, and it was then properly sealed. Each measurement lasted 90 s and the CO_2 flux was derived by fitting an exponential curve on the CO_2 mixing ratio evolution inside the closed chamber measured at a frequency of 1 Hz.[45,46] All measurements were taken under artificial white light (85 μmol m^{-2} s^{-1}) and relatively constant temperature and CO_2 concentration (20.7 ± 0.9 °C and 606 ± 50 μmol mol^{-1}, respectively). In the post-processing phase, data were handled using SoilFluxPro® software to adjust the volume of the system to the modified chamber and to set the dead band interval to 10 s to ensure the establishment of a steady mixing of CO_2 before the beginning of the measurements (Licor 2010, Fig. S11b). Only fluxes with $R^2 > 0.60$ and originated by non-contaminated plates were kept for further analysis. The quality check process carried out on the gas exchange measurements caused the removal of two out of five measured plates for both CTRL and P3HT-NPs treated plates. One CTRL plate was excluded due to the contamination of the plate with a bacterial colony, while one plate of CTRL and two plates of P3HT-NPs treated plants were removed because the coefficient of determination of the flux was below the fixed threshold of 60%. Thus, 10 plants over 3 plates were considered as the CTRL samples. 16 plants over 3 plates were considered as the P3HT-NPs samples. Data were analysed *via* OriginPro 2021.

Hyperspectral images

Hyperspectral images (HSIs) were acquired *via* HERA hyperspectral camera (NIEROS). Images were captured using an exposure time of 3 ms and a white LED as the light source to illuminate the field of view of the camera. The distance between the sample and the camera was 120 cm. The spectral range was 400–1000 nm. Data acquisition and management were conducted using HERA_analysis_APP (NIEROS). Based on the Fourier-transform approach, the spectrum of light at different selected pixels of the CTRL, Si-NPs and P3HT-NPs plant leaves was measured. HSIs were processed using ENVI 5.3 (Exelis, McLean, VA, USA), and the ROI tool was used to draw a region of interest corresponding to the measurement area of the leaf.

3 leaves per plant, 5 plants per condition were considered. Data were analysed *via* OriginPro 2021.

Confocal imaging

Leaves were freshly detached from the plant and fixed by using coverslip glass. The imaging acquisition was made by using a Leica SP8-X confocal microscope with 63x oil immersion objective. The P3HT-NPs were detected by using the 520 nm excitation wavelength and the stomata cells with 488 excitation wavelengths.

Results and discussion

Light harvesting nanoparticles to develop biohybrid plants

Biohybrid plants have been obtained by sowing *A. thaliana* seeds into Murashige and Skoog salt (MS) agarose-based hydrogel medium[47] supplemented with P3HT-NPs. MS medium and MS medium supplemented with silica NPs (Si-NPs) were used as controls (CTRL). Si-NPs were used as a negative control due to their comparable size to P3HT-NPs but lack of photoactive properties. The plant growth observation period was 19 days. Biosafety and growth-promoting effects of P3HT-NPs on *A. thaliana* plants were investigated, as well as potential negative effects (*e.g.*, pH variation of the agarose-based hydrogel supplemented medium).

P3HT-NPs preparation and characterization. P3HT-NPs were obtained *via* nanoprecipitation method. The 152.3 ± 64 nm measured hydrodynamic diameter (Fig. 1a) allows NPs to be uptaken *via* plant roots.[48] The measured zeta potential (−41.2 ± 6.2 mV) and the polydispersity index (PdI = 0.158, Fig. 1a, inset) indicate a stable colloidal suspension.[49] Furthermore, the negative zeta potential facilitates NPs penetration (from the root surface to the vascular system) and transport (from root to shoot).[50]

The absorption and emission spectra of P3HT-NPs (Fig. 1b and Fig. S1b) feature peaks at 516 and 655 nm, respectively. Notably, the absorbance spectrum of P3HT-NPs, spanning from 450 to 650 nm, aligns with the spectral region where chlorophyll exhibits minimal absorption in plants (Fig. 1b). Conversely, the emission spectrum of P3HT-NPs, extending from 600 to 750 nm, coincides with the pronounced absorption spectral range of the plant's chlorophyll (Fig. 1b). These spectral properties substantiate the theoretical potential for employing P3HT-NPs as photonic antennas to augment plant light absorption. Absorbance and emission spectra show the P3HT-NPs retention of optical properties following dialysis process and sterilization (Fig. S1b), which are essential preparatory steps for biological application, with minor shifts indicative of morphological or aggregation changes during processing. This confirms the optical stability of the P3HT-NPs in biologically relevant conditions. Morphological investigation of P3HT-NPs through scanning electron microscopy (SEM) imaging (Fig. 1c) corroborated the dimensions and geometry of the NPs. Additionally, high-resolution scanning/transmission electron microscopy (S/TEM) analysis verified that the NPs shape and structural integrity were preserved throughout the preparation and processing steps, including dialysis and sterilization (Fig. S2a–c). Finally, to assess the chemical integrity of

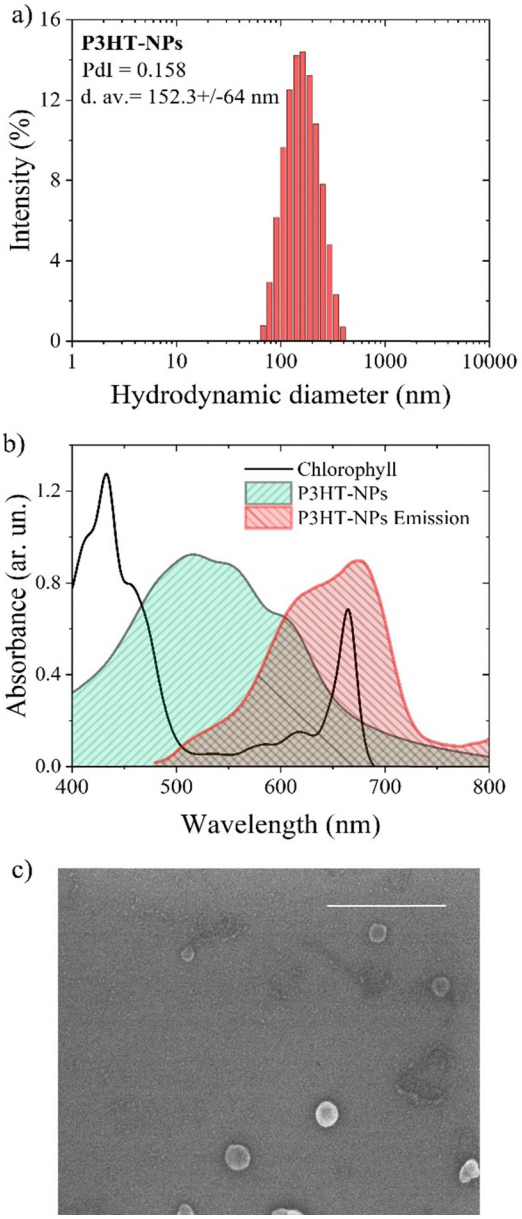

Fig. 1 P3HT-NPs characterization. (a) Hydrodynamic diameter distribution of P3HT-NPs, measured *via* dynamic light scattering (DLS). The plot illustrates the size dispersion of P3HT-NPs in solution, highlighting the predominant hydrodynamic diameter range, indicative of the nanoparticles' stability and uniformity in aqueous environments. The polydispersity index (PdI) and average diameter (d. av.) are reported as inset. (b) Spectral match of P3HT-NPs with chlorophyll extracted from *Arabidopsis thaliana* leaves (see Methods). The absorption (shaded light green) and emission (shaded red) spectra of P3HT-NPs are shown alongside within the absorption spectra of chlorophyll (black line). The figure highlights potential interactions in the 450–650 nm range for P3HT absorption and 650–700 nm for P3HT emission, suggesting the capacity of P3HT-NPs to interact with chlorophyll-based photosynthetic processes. (c) Scanning electron microscopy (SEM) of P3HT-NPs showing the morphology and size of P3HT-NPs with uniform geometry and nanoscale dimensions. Scale bar is 500 nm.

the sterilized P3HT-NPs, those used in subsequent experiments for plant integration, scanning photoelectron microscopy (SPEM) and X-ray photoelectron spectroscopy (XPS) analyses were conducted. SPEM chemical maps, along with the corresponding XPS micro-spectra, confirmed the presence of characteristic carbon (C1s) and sulfur (S2p) signals associated with the P3HT backbone, located at the binding energies of approximately 285 eV and 163 eV, respectively (Fig. S3). Additional ultraviolet photoelectron spectroscopy (UPS) confirmed a work function of 3.4 eV for the sterile P3HT-NPs with the highest occupied molecular orbital (HOMO) onset at $\sim$1.5 eV below the Fermi energy, in accordance with the literature[51] (Fig. S4). These values are consistent with the known chemical composition of poly(3-hexylthiophene),[52] confirming the stable morphological and chemical structure of the P3HT-NPs, and thus their suitability for application in biohybrid plant systems.

P3HT-NPs biosafety and growth-promoting evaluation in *Arabidopsis thaliana*. To study the biosafety of P3HT-NPs on plant systems an MS agarose-based hydrogel medium (CTRL) was combined with the P3HT-NPs at different concentrations (P3HT-NPs [0.01 mg mL^{-1}], [0.05 mg mL^{-1}] and [0.10 mg mL^{-1}]). Sterile *A. thaliana* seeds were sown both in the CTRL and in the P3HT-NP supplemented media. The samples were then placed in a plant growth chamber, following day (full spectrum white light, Fig. S5a)/night (dark) cycles for 9 days.

At the initial germination checkpoint (T_0, 3 days after incubation within the plant growth chamber), all germinated samples uniformly measured approximately 1 cm in root length, exhibiting no evident size variations between the CTRL and the P3HT-NPs-treated samples (Fig. S6). Remarkably, by the 9th day post-germination (T_{end}, 12 days following incubation), *A. thaliana* plants treated with the highest concentration of P3HT-NPs ([0.10 mg mL^{-1}]) showed a 45% increase in root length (8.10 $\pm$ 0.99 cm) compared to the CTRL (5.56 $\pm$ 2.07 cm) (Fig. 2a and b). Additionally, the P3HT-NPs [0.10 mg mL^{-1}] treated plants demonstrated a leaf area expansion of 1.0 $\pm$ 0.3 mm^2 beyond that of the CTRL (Fig. 2c and d), and a 0.03 $\pm$ 0.02 mg increase in dry weight (Table 1) indicative of a 11% enhancement in biomass production. No evident differences in the dry weight were observed under conditions with P3HT-NPs at lower concentrations (Table 1).

While some variability is inherent in biological systems, these findings support the biosafety of P3HT-NPs, as indicated by the unaltered plant phenotype (Fig. 2b) and the positive plants growth-promoting both for roots and leaves.

Fluorescence microscopy analysis was employed to assess the persistence of P3HT-NPs within the MS agarose-based hydrogel medium at T_{end}. After a 20-day integration period, the P3HT-NPs retained their fluorescence properties (Fig. S7), underscoring their stability and enduring efficacy in the medium.

P3HT-NPs effect on plant growth and photosynthetic enhancement in *Arabidopsis thaliana*. Motivated by the promising preliminary findings, a subsequent experiment was conducted to further exploit the impact of P3HT-NPs on plants. MS agarose-based hydrogel medium supplemented with P3HT-NPs ([0.10 mg mL^{-1}]) was prepared as previously described and selected for evaluation. Control groups included MS medium (CTRL), and Si-NPs supplemented medium, both prepared following identical protocols. The experimental observation period was 19 days.

Evaluation of stability, reactive oxygen species formation and pH variations of MS medium supplemented with P3HT-NPs. To evaluate potential alteration in the optical properties of P3HT-NPs in MS medium after 19 days of light exposure under day/night cycles, absorbance spectra were measured for CTRL, Si-NPs, and P3HT-NPs media at T_{start} (day of preparation) and T_{end} (day 19). No significant differences were observed in the spectra, with an overall 20% decrease in absorbance across all samples over the period (Fig. S8). For the P3HT-NPs medium, absorbance in the 450–500 nm range was evident at both time points, reflecting the presence of P3HT-NPs.

To investigate the formation of reactive species resulting from the oxygen reduction reaction on P3HT,[53] H_2O_2 and pH measurements were performed on CTRL, Si-NPs and P3HT-NPs supplemented media at T_{start} and T_{end}. No significant variation in H_2O_2 levels (Fig. S9), or pH values (Table S1) were noticed, excluding any significant chemical modification, potentially harmful to the plants, in the P3HT-NPs supplemented medium.

Germination and growth of *A. thaliana* in P3HT-NPs supplemented media. At T_0 (germination checkpoint), only 14, 0, and 15 plants over 60 seeds sown into CTRL, Si-NPs, and P3HT-NPs supplemented media germinated, respectively. All the germinated samples uniformly measured approximately 1 cm in root length, exhibiting no evident variation (Fig. S10). At T_3 (day 13th within the growth chamber) (Fig. 3a) and at T_{end} an appreciable increase in root length of 25–26% and 91–92% was noted in *A. thaliana* seeds sown and cultivated within the medium incorporating P3HT-NPs (root lengths: 7.22 $\pm$ 0.58 cm at T_3 and 9.53 $\pm$ 0.59 cm at T_{end}) in comparison to the CTRL (root lengths: 5.76 $\pm$ 1.25 cm at T_3 and 7.55 $\pm$ 1.26 cm at T_{end}) and Si-NPs supplemented medium (root lengths: 3.77 $\pm$ 0.77 cm at T_3 and 4.97 $\pm$ 1.95 cm at T_{end}) respectively (Fig. 3b). P3HT-NPs growth-promoting also allowed 17% (at T_{end}) increase in biomass production, per plant, respect to CTRL when considering normalized leaves dry weights, as detailed in Table 2.

These findings confirm and reinforce the growth-promoting effects of P3HT-NPs observed in previous results also providing evidence of the inhibitory effect of Si-NPs on plant growth.

Consistently with the root length increment, the leaf area measured at T_{end} (Fig. 3c) of P3HT-NPs treated plants (0.09 $\pm$ 0.03 cm^2) was larger by factors of 1.5 and 1.8 respect to the CTRL (0.06 $\pm$ 0.01 cm^2) and Si-NPs (0.05 $\pm$ 0.02 cm^2) treated plants.

Representative pictures of *A. thaliana* plants grown in P3HT-NPs supplemented medium and of plant leaves from each treatment group are depicted in Fig. 3d and e.

P3HT-NPs light antennas in *Arabidopsis thaliana*. To further investigate the growth-promoting effects of P3HT-NPs and their ability to act as light antennas by broadening the absorption

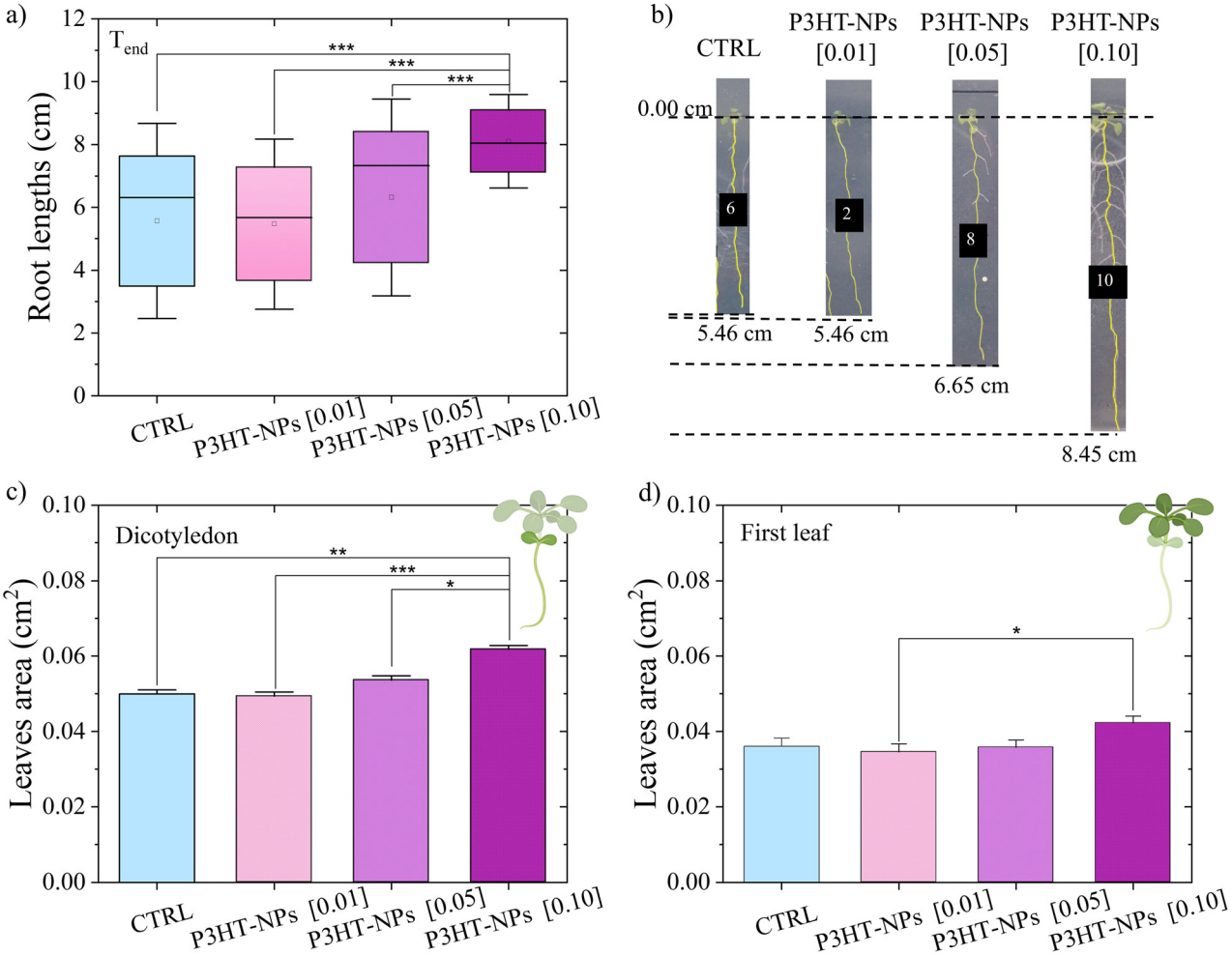

Fig. 2 P3HT-NPs growth-promoting evaluation in *Arabidopsis thaliana*. (a) Root lengths at the end of the experimental period (T_{end}, 9 days post-germination, 12 days after incubation), measured for plants grown in MS agarose-based hydrogel soil (CTRL) and MS agarose-based hydrogel soil supplemented with P3HT-NPs at different concentration (0.01 mg mL^{-1}, 0.05 mg mL^{-1}, 0.10 mg mL^{-1}). Error bars represent the standard deviation (SD). (b) Representative pictures for roots growth comparison with a scale reference between CTRL and treated groups. (c) Leaf area measurements for dicotyledon (first embryonic leaves) and (d) for first leaf (first photosynthetic leaf that develops after the dicotyledons), across the same treatment groups, highlighting the effects of NPs concentration on plant leaves development. Error bars represent the standard error (SE). Statistically (one-way ANOVA) significant differences between groups are indicated by asterisks: *$p < 0.05$, **$p < 0.01$, ***$p < 0.001$.

Table 1 Dry weight of *Arabidopsis thaliana* plants grown across different treatments. Average of dry weight (mg) for *A. thaliana* plants grown in MS agarose-based hydrogel medium (CTRL) and MS medium supplemented with P3HT-NPs at different concentrations ([0.01 mg mL^{-1}], [0.05 mg mL^{-1}], [0.10 mg mL^{-1}]). Values are expressed as the normalized leaves dry weight (mg per plants) mean ± SD

Samples	Mean (mg)
CTRL	0.28 ± 0.02
P3HT-NPs [0.01 mg mL^{-1}]	0.26 ± 0.02
P3HT-NPs [0.05 mg mL^{-1}]	0.28 ± 0.03
P3HT-NPs [0.10 mg mL^{-1}]	0.31 ± 0.02

spectrum of plants, *A. thaliana* plants were grown in CTRL, and P3HT-NPs supplemented media within a growth chamber for 9 days. The plants were subjected to standard day/night cycles (as previous experiments) and day/night cycles with additional 4 hours of green light (Fig. S5b). 9 days post-germination, an increase in root length of 27% and 31% was observed in *A. thaliana* grown in the P3HT-NPs supplemented medium compared to the CTRL, under standard conditions and with the addition of 4 hours of green light, respectively (Fig. 3f and g).

These results corroborate the positive effect of P3HT-NPs on root growth suggesting that the presence of P3HT-NPs also enables the plants to absorb green light.

Analysis of photosynthesis, optical properties, and nanoparticle localization in biohybrid plants

The photosynthetic capacity of *A. thaliana* plants grown in CTRL and P3HT-NPs supplemented media was investigated at T_{end}. Plant photosynthetic efficiency and the overall carbon balance were investigated by measuring the net CO_2 assimilation (balance between CO_2 fixation and CO_2 production by photorespiration). Si-NPs supplemented medium was not considered due to bacterial colony contamination, which could

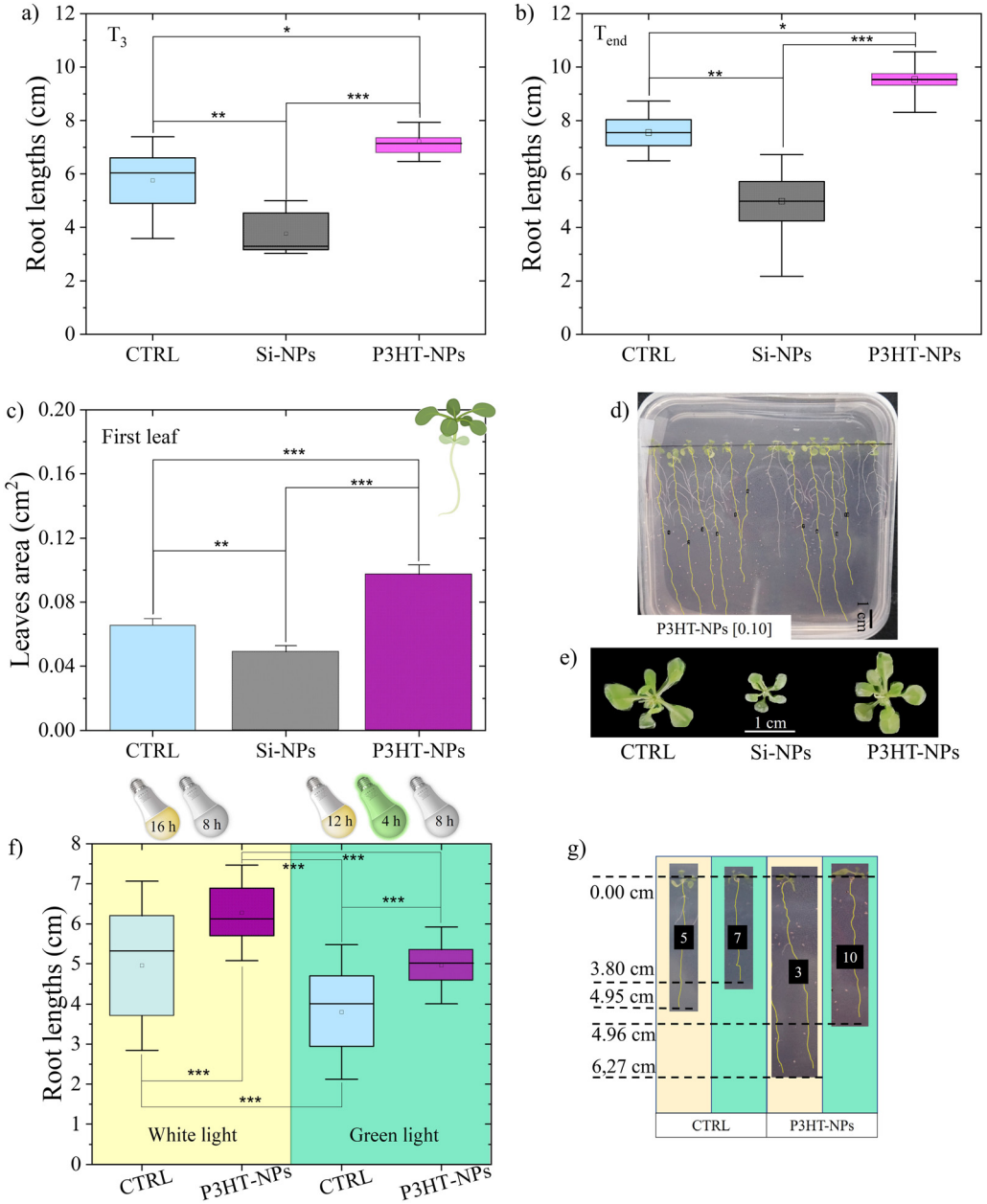

Fig. 3 P3HT-NPs growth-promoting evaluation in *Arabidopsis thaliana*. (a) Root lengths at the 13th day within the growth chamber (T_3), measured for plants grown in MS agarose-based hydrogel medium (CTRL) and MS medium supplemented with Si-NPs, and P3HT-NPs [0.10 mg mL^{-1}]. (b) Root lengths at the end of the experimental period (T_{end}, 19 days post-germination), measured for plants grown across the different treatments. Error bars represent the SD. (c) Comparison of the first leaf area (cm^2) for plants grown across the different treatments. Error bars represent SE. (d) Representative picture of plants grown in P3HT-NPs supplemented medium. (e) Representative pictures of the plants from each treatment group, visually highlighting the differences in leaf size. (f) Root lengths for CTRL and P3HT-NPs treated plants grown under standard white light (yellow shaded area) and white light with additional green light (green shaded area). Error bars represent the SD. (g) Representative images of the root systems, with measurements indicating the increase in root length. Statistically significant differences between groups (one-way ANOVA) are indicated by asterisks: *$p < 0.05$, **$p < 0.01$, ***$p < 0.001$.

interfere with CO_2 assimilation processes. Samples were collected from the growth chamber, placed in a sealed custom-made gas-exchange transparent chamber and illuminated with a full-spectrum white light mimicking solar radiation as shown in Fig. S11a. P3HT-NPs treated plates have shown a cumulative increase in shoot biomass by 42% with respect to the CTRL plates (4.53 ± 0.28 *vs.* 3.20 ± 0.24 mg of dry weight, Fig. 4a and Table S2). In P3HT-NPs *A. thaliana* treated plants the net CO_2 assimilation increased by 11% respect to the CTRL (2.30 *vs.* 2.07 nmol of CO_2 plate^{-1} s^{-1}, Fig. 4b and Table S2). These results represent a first attempt to measure the assimilation capacity of P3HT-NPs engineered *A. thaliana* plants and support the possible positive effects of the treatment on the photosynthetic activity of the plant.

Table 2 Dry weight of *Arabidopsis thaliana* plants grown across different treatments. This table presents the average dry weight (mg) of *A. thaliana* plants grown in MS agarose-based hydrogel medium (CTRL) and MS medium supplemented with Si-NPs and P3HT-NPs (at a concentration of 0.10 mg mL^{-1}). Values are expressed as the normalized leaves dry weight (mg per plants) mean ± SD

Samples	Mean (mg)
CTRL	0.71 ± 0.07
Si-NPs [0.10 mg mL^{-1}]	0.61 ± 0.05
P3HT-NPs [0.10 mg mL^{-1}]	0.83 ± 0.06

To evaluate the effects of P3HT-NPs on plant physiology, hyperspectral imaging (HSI) was used alongside standard morphological characterization. This non-destructive technique captures high-resolution spectral reflectance (400–1000 nm), thereby enabling analysis of leaf pigments, nutrient status, stress responses, and photosynthesis.[54] Spectral curves of leaves from *A. thaliana* plants grown in CTRL, Si-NPs, and P3HT-NPs media showed significant differences in the 500–650 nm range, with P3HT-NPs treated plants exhibiting 3 times higher reflectance than controls (Fig. 4c) while the reflectance between 800 and 450 nm was similar for the CTRL and Si-NPs samples. Selected regions of interest (ROIs) are shown in Fig. S12. This augmentation suggests a specific interaction between P3HT-NPs and plant tissues, potentially influencing light absorption and utilization, warranting further study of nanomaterial–plant interactions.

Finally, confocal images (Fig. S13, S14 and Fig. 4d) of differently treated samples of *A. thaliana* reveal distinct features and enable the following considerations: (i) red fluorescence is observed between guard cells in all the samples and attributed to chlorophyll autofluorescence[55] (Fig. S13 and Fig. 4d); (ii) in contrast intense red spots, measuring less than 1 μm in diameter, were observed exclusively in the leaves of the plants grown in the P3HT-NPs supplemented medium. The observed fluorescent features may result from individual P3HT-NPs or small aggregates formed post-uptake, anyway indicative of the presence of P3HT in the leaf; (iii) confocal images of P3HT-NPs supplemented medium and roots of *A. thaliana* plants grown in it (Fig. S14) further confirm the potential uptake of P3HT-NPs by the root tissues. Taken together, these observations strongly suggest that P3HT-NPs, introduced through the supplemented medium, were effectively absorbed by the roots and transported to the leaves *via* the stem. Their localization in the leaves corroborates the hypothesis of their role as light-harvesting antennas, enhancing plant growth, reflectance, and photosynthetic activity.

Conclusions

For the first time, we present the successful development of enhanced biohybrid plants through the natural incorporation of P3HT-NPs into the *A. thaliana* 3D organization, *in vivo*.

The improved growth and biomass production of P3HT-NPs biohybrid plants indirectly indicate enhanced photosynthetic activity, confirmed by net CO_2 assimilation measurements showing 11% higher CO_2 utilization than CTRL plants. This suggests that P3HT-NPs, transported to leaves, act as photonic antennas, boosting light absorption and influencing electron-transfer chain reactions (the light-dependent reaction, eqn (I)) taking place in the reaction centre of the chlorophyll,[56] as represented in Fig. 5a. During the photosynthesis sunlight energy energizes an electron in the green organic pigment chlorophyll, enabling the electron to move along an electron-transport chain in the thylakoid membrane.[57] Indeed, it is well-established that CPs can efficiently transfer excitons to adjacent low-energy acceptors, analogous to the energy transfer observed between antenna pigments in photosynthesis.[58] It is worth noticing that chlorophyll, and all photosynthetic pigments, possess long-range conjugated π-electron systems[59] similar to those found in CPs. In a first approximation, the relative energy alignment of the HOMO and lowest unoccupied molecular orbital (LUMO) levels of P3HT-NPs and chlorophyll provides insight into the potential for electron transfer within the system (Fig. 5b and c). To visualize this alignment, we determined the energy levels of P3HT-NPs using our UV-Vis and UPS measurements (see Fig. S1, S3 and S4), as shown in Fig. 5b. The energy levels of chlorophyll (Chl *b*) were taken from Mondal *et al.*,[60] and are also included in Fig. 5b. Although the constructed energy diagram does not account for possible distortions due to the local environment, it clearly indicates that photoexcitation (*e.g.*, by sunlight) could promote electron transfer from P3HT-NPs to chlorophyll. This is supported by the relatively small energy offset of approximately 0.2 eV between the LUMO levels of P3HT-NPs and chlorophyll.

Therefore, the presence of P3HT-NPs in the leaves might allow the biohybrid plant to absorb a broader range of light, generating more electrons in the electron-transport chain within photosystem II (PSII, the protein complex in chloroplasts involved in photosynthesis process) increasing the charges transfer and generating more electronic holes by the absorbed light, thus enhancing the photoelectric conversion efficiency. Therefore, it may lead to an augment photosynthesis beyond natural chloroplasts.

HIS analysis revealed higher reflectance in the green region for P3HT-NPs treated leaves, suggesting increased chlorophyll content or improved chloroplast activity, aligning with observed photosynthetic and biomass gains, further supporting the hypothesis of P3HT-NPs acting as photonic antennas when transported and located into plant leaves, as confirmed by confocal imaging.

These findings demonstrate the potential of P3HT-NPs for biohybrid plant creation, opening avenues for agricultural and environmental applications. Although P3HT-NPs have demonstrated biocompatibility with *A. thaliana*, future work will be necessary to assess their environmental fate including studies on persistence in soil and water and their long-term interactions with ecosystems. This work introduces biohybrid-photosynthetic living systems, reinforced with light-harvesting nanomaterials, as a novel strategy to enhance photosynthesis and bioenergy production paving the way for significant advancement in plant bio-nanotechnology.

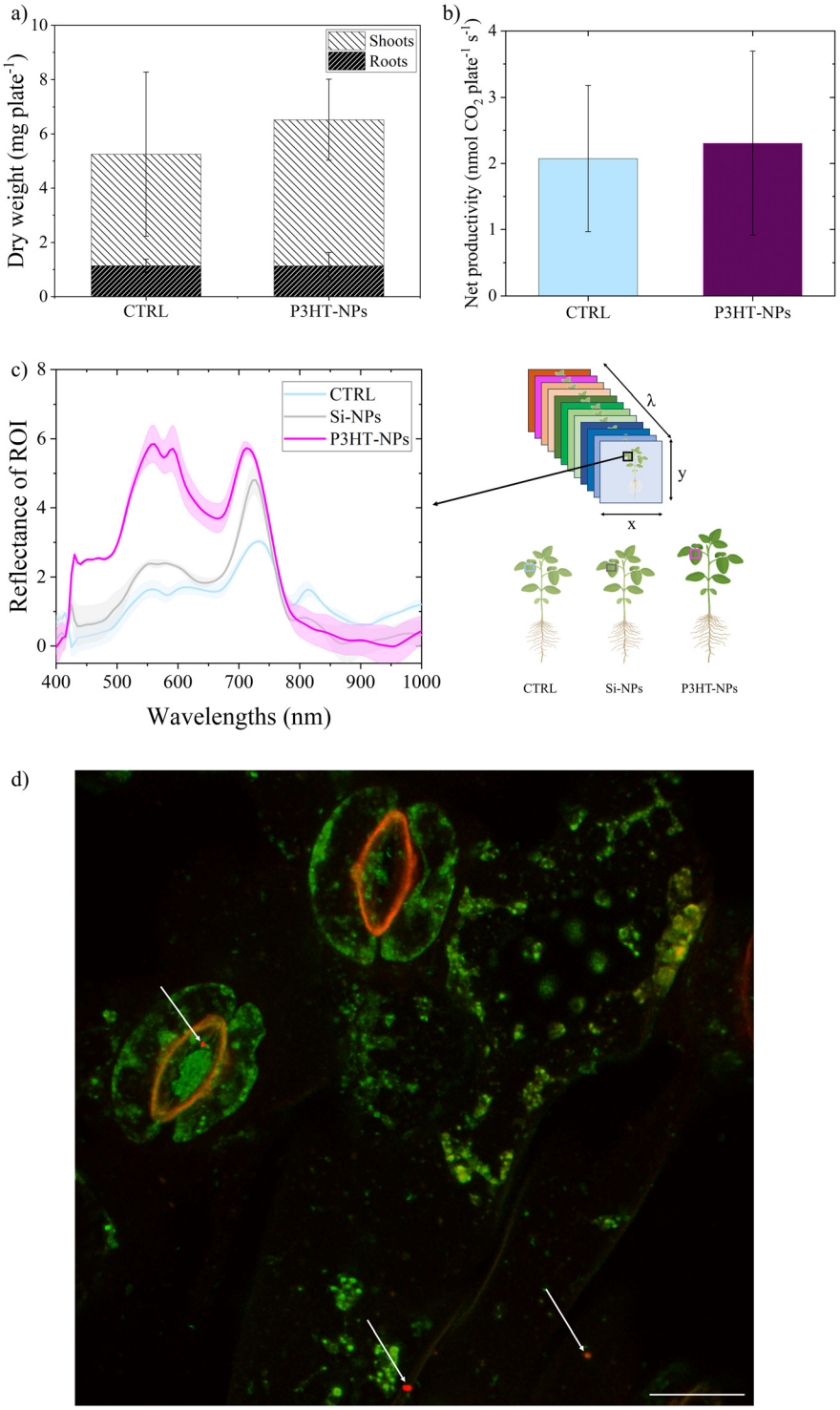

Fig. 4 Photosynthetic capacity and optical characterization of *Arabidopsis thaliana* plants grown across different treatments. Comparison of the biomass (a) and the net productivity (b) (equal to net CO_2 assimilation, nmol CO_2 plate^{-1} s^{-1}) between plants grown in MS agarose-based hydrogel soil (CTRL) and MS medium supplemented with P3HT-NPs (at a concentration of 0.10 mg mL^{-1}). The roots and shoots dry weight and the net productivity values are reported per plate. Error bars represent the SD. (c) Hyperspectral analysis of leaf reflectance. The spectral curves represent the reflectance spectra of regions of interest (ROIs) on leaves across various wavelengths, with the average shown as a continuous line and the SD as shaded areas, for plants grown in CTRL and Si-NPs and P3HT-NPs (at a concentration of 0.10 mg mL^{-1}) supplemented media, as illustrated schematically on the right. The hyperspectral data cube linked to the measured leaves spectral signature is also represented, as well as a representation of the different analysed samples. (d) Fluorescence confocal microscopy of *Arabidopsis thaliana* leaves. Images of plants grown in P3HT-NPs supplemented medium. The natural autofluorescence of chlorophyll is appreciable, while the presence of P3HT-NPs as distinct red fluorescence spots (indicated by arrows) is highlighted. These intense red spots, less than 1 μm in diameter, confirm the uptake and translocation of P3HT-NPs from roots to leaves. Scale bars 10 μm.

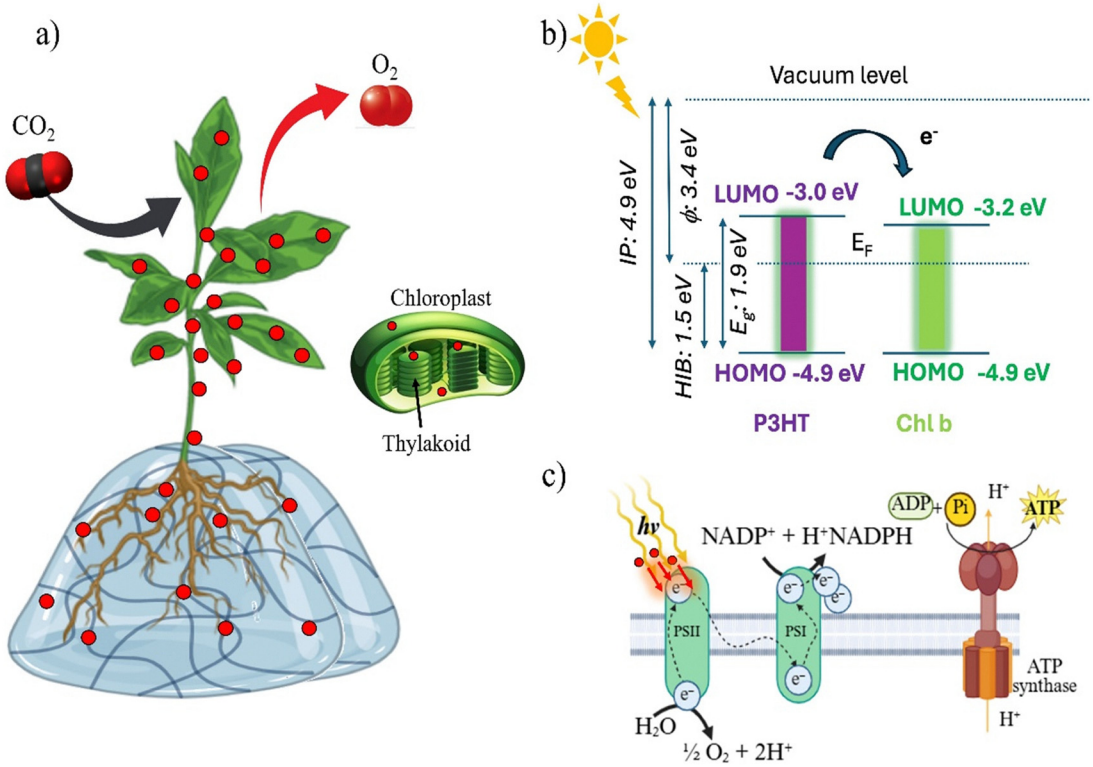

Fig. 5 Schematic representation of the mechanism of photosynthetic enhancement in biohybrid plants incorporating P3HT-NPs. (a) Illustration of P3HT-NPs (red circles) uptake from the hydrogel-based medium, root internalization, and translocation to leaves, where they localize in chloroplasts. (b) Energy level diagram comparing the HOMO and LUMO positions of P3HT-NPs and chlorophyll *b* (Chl *b*). Data for P3HT-NPs were experimentally determined *via* UPS and UV-Vis (Ionization potential (IP) = 4.9 eV, work function (ϕ) = 3.4 eV, hole injection barrier (HIB) = 1.5 eV), and Chl *b* values were taken from literature. The relative alignment of energy levels suggests potential photo-induced electron transfer from excited P3HT-NPs to chlorophyll, enhancing charge separation efficiency. (c) Conceptual depiction of the interaction between P3HT-NPs and the photosynthetic electron transport chain within the thylakoid membrane. P3HT-NPs act as photonic antennas, absorbing light and facilitating electron injection into photosystem II (PSII) and PSI, leading to increased photosynthetic activity of the biohybrid plants and subsequent increased CO_2 assimilation.

Future studies should aim to optimize the concentration and delivery methods of NPs into plants and to further elucidate the mechanisms underlying the NPs/living system interactions. Particular emphasis should be placed in analysing chlorophyll fluorescence-based photosynthetic parameters, such as electron transport rates (ETR), to gain deeper insights into the effects of NPs on the light-dependent reactions of photosynthesis. In addition, subcellular localization through TEM and chlorophyll fluorescence lifetime measurements may help clarify nanoparticle interactions at the organelle level, providing direct mechanistic evidence of their role in enhancing photosynthesis.

Author contributions

M. C.: conceptualization, data curation, formal analysis, investigation, methodology, validation, visualization, supervision, writing – original draft. M. M.: data curation, formal analysis, validation, writing – review & editing. C. A.: data curation, methodology. D. Z.: data curation, formal analysis, validation, investigation. S. K.: methodology, writing – review & editing. A. O.: data curation, formal analysis, validation. T. R.: investigation, data curation, writing – review & editing. S. W.: data curation. T. F.: data curation. G. G.: data curation, validation, writing – review & editing. A. L.: data curation, formal analysis, validation. P. I.: writing – review & editing. Z. M.: formal analysis, investigation. M. T.: formal analysis, validation, investigation, resources, writing – review & editing. M. V. N.: formal analysis, validation, investigation, resources, writing – review & editing. A. P.: formal analysis, investigation, methodology. A. G.: supervision, resources, writing – review & editing. P. L.: supervision, resources. F. C.: supervision, resources, writing – review & editing. D. L.: conceptualization, supervision, resources, writing – review & editing. T. M.: conceptualization, supervision, resources. L. P.: conceptualization, funding acquisition, supervision, writing – review & editing. All the authors discussed the results and commented on the paper.

Conflicts of interest

There are no conflicts to declare.

Data availability

The data underpinning the findings of this study are available within the article and its SI.

Chlorophyll structure and P3HT-NPs optical properties at different processing stages. High-resolution scanning/transmission electron microscopy (S/TEM) images in transmission mode of P3HT-NPs at different processing stages. Chemical properties of sterilised P3HT-NPs. Electronic properties of sterilised P3HT-NPs. Light spectrum distribution of the illumination light sources in the plant growth chamber. Figures of investigated plants (CTRL and P3HT-NPs supplemented) at initial germination checkpoint. Fluorescent Microscopy of P3HT-NPs in the agarose-based hydrogel soil. Absorbance spectra of MS medium and MS media supplemented with P3HT-NPs and Si-NPs. H_2O_2 evaluation in the media. Media pH evaluation. Description of the photosynthetic activity experimental set-up. Summary table for sample plates and number of plants considered for the CO_2 assimilation measurements. Hyperspectral imaging of *Arabidopsis thaliana* plants grown under different treatments. Fluorescence Confocal Microscopy of *Arabidopsis thaliana* leaves. See DOI: **https://doi.org/10.1039/d5mh00341e**

Acknowledgements

This research was supported by the educational-academic fundings of the Free University of Bozen-Bolzano and Senslab (sensing laboratory) project. This work was partially supported by the European Union Next-GenerationEU (PIANO NAZIONALE DI RIPRESA E RESILIENZA (PNRR) – Missione 4, Componente 1, Investimento 4.1 – D.M. 351/2022) and Missione 4 Componente 2, Iinvestimento 3.3 – Decreto del Ministero dell'Università e della Ricerca n.352 del 09/04/2022) and by Fondazione Bruno Kessler (co-financing this project) within the Advanced Systems Engineering PhD Program at UniBZ. This research was also supported by the project PMDI (EFRE1030), co-financed by the European Union within the Regional Development Fund (ERDF} Programme 2021–2027. This research was also partially funded by the Italian MUR under PRIN 2022 Project '2D-EMMA' (Project n. 202289PMBP, CUP: B53D23004010006) and under PRIN 2022 Project 'PETRA' (Project n. 2022T7ZSEK, CUP B53D23001860006) in the frame of Next Generation EU. M. Ciocca would like to acknowledge the technicians at the University of Bozen-Bolzano (namely F. Valentinuzzi, M. Ventura, C. Ceccon, M. Malavasi) for their invaluable assistance throughout the experimental work. Their expertise and dedication were instrumental in the successful completion of this research. M. Ciocca also thanks D. Asensio for the valuable discussions and insights into the measurements of photosynthetic activity in plants, which greatly contributed to this work. M. Ciocca also extends her gratitude to Prof. M. Tagliavini for his support, providing connections for tests and measurements, as well as for the insightful discussions on plant photosynthetic activity measurements. M. Ciocca would like to acknowledge Prof. O. Lanz for the support in the hyperspectral image experiments. In addition, Dr L. Gregoratti and Dr M. Amati are gratefully acknowledged for the support during the SPEM sessions at the ESCA microscopy beamline at ELETTRA (proposal no. 20245205). The authors thank the Department of Innovation, Research, University and Museums of the Autonomous Province of Bozen/Bolzano for covering the Open Access publication costs.

References

1 M. D. Archer and J. Barber, *Molecular to Global Photosynthesis*, 2004, 1–41.
2 N. Chaffey, B. Alberts, A. Johnson, J. Lewis, M. Raff, K. Roberts and P. Walter, Molecular biology of the cell, *Annals of Botany*, 4th edn, 2003, vol. 91, p. 401.
3 S. C. Bhatla and M. A. Lal, *Plant Physiology, Development and Metabolism*, Springer Nature, Singapore, 2023, pp. 107–154.
4 I. McConnell, G. Li and G. W. Brudvig, Energy Conversion in Natural and Artificial Photosynthesis, *Chem. Biol.*, 2010, **17**, 434–447.
5 G. Farré, S. Gómez-Galera, S. Naqvi, C. Bai, G. Sanahuja, D. Yuan and C. Zhu, in *Encyclopedia of Sustainability Science and Technology*, ed. R. A. Meyers, Springer, New York, 2012, pp. 7902–7932.
6 J. K. Hoober, L. L. Eggink and M. Chen, Chlorophylls, ligands and assembly of light-harvesting complexes in chloroplasts, *Photosynth. Res.*, 2007, **94**, 387–400.
7 P. Ghosh, P. Das, R. Mukherjee, S. Banik, S. Karmakar and S. Chatterjee, Extraction and quantification of pigments from Indian traditional medicinal plants: A comparative study between tree, shrub, and herb, *Int. J. Pharm. Sci. Res.*, 2018, **9**, 3052–3059.
8 K. E. Redding and S. Santabarbara, Photosystems I and II, The Chlamydomonas Sourcebook, *Organellar and Metabolic Processes*, 2023, vol. 2, pp. 525–560.
9 J. R. Bolton and D. O. Hall, Photochemical Conversion and Storage of Solar Energy, *Annu. Rev. Environ. Resour.*, 1979, **4**, 353–401.
10 J. He and C. Janáky, Recent Advances in Solar-Driven Carbon Dioxide Conversion: Expectations versus Reality, *ACS Energy Lett.*, 2020, **5**, 1996–2014.
11 S. Molinari, R. F. Tesoriero and C. M. Ajo-Franklin, Bottom-up approaches to engineered living materials: Challenges and future directions, *Matter*, 2021, **4**, 3095–3120.
12 T.-C. Tang, B. An, Y. Huang, S. Vasikaran, Y. Wang, X. Jiang, T. K. Lu and C. Zhong, Materials design by synthetic biology, *Nat. Rev. Mater.*, 2021, **6**, 332–350.
13 X. Yuan, H. Xu, X. Liu, J. Zhang, J. Li, Q. Liang, B. An, G. M. Paternò, M. Zhang, Y. Tang, C. Zhang, D. Xu, C. Zhong, K. Li and X. Wang, Engineered Living Energy Materials, *Interdiscip. Mater.*, 2025, **4**, 412–455.
14 G. M. Newkirk, P. de Allende, R. E. Jinkerson and J. P. Giraldo, Nanotechnology Approaches for Chloroplast Biotechnology Advancements, *Front. Plant Sci.*, 2021, **12**, 691295.
15 W. Xiong, Y. Peng, W. Ma, X. Xu, Y. Zhao, J. Wu and R. Tang, Microalgae–material hybrid for enhanced photosynthetic energy conversion: a promising path towards carbon neutrality, *Natl. Sci. Rev.*, 2023, **10**, nwad200.

16 Y. Yang, M. A. Zwijnenburg, A. M. Gardner, S. Adamczyk, J. Yang, Y. Sun, Q. Jiang, A. J. Cowan, R. S. Sprick, L.-N. Liu and A. I. Cooper, Conjugated Polymer/Recombinant *Escherichia coli* Biohybrid Systems for Photobiocatalytic Hydrogen Production, *ACS Nano*, 2024, **18**, 13484–13495.
17 G. M. Paternò, Materials-driven strategies in bacterial engineering, *MRS Commun.*, 2024, **14**, 1027–1036.
18 G. Tullii, F. Gobbo, A. Costa and M. R. Antognazza, A Prototypical Conjugated Polymer Regulating Signaling in Plants, *Adv. Sustain. Syst.*, 2022, **6**, 2100048.
19 C. Routier, L. Vallan, Y. Daguerre, M. Juvany, E. Istif, D. Mantione, C. Brochon, G. Hadziioannou, Å. Strand, T. Näsholm, E. Cloutet, E. Pavlopoulou and E. Stavrinidou, Chitosan-Modified Polyethyleneimine Nanoparticles for Enhancing the Carboxylation Reaction and Plants' CO2 Uptake, *ACS Nano*, 2023, **17**, 3430–3441.
20 F. Yang, C. Liu, F. Gao, M. Su, X. Wu, L. Zheng, F. Hong and P. Yang, The Improvement of Spinach Growth by Nano-anatase TiO2 Treatment Is Related to Nitrogen Photoreduction, *Biol. Trace Elem. Res.*, 2007, **119**, 77–88.
21 R. Doshi, W. Braida, C. Christodoulatos, M. Wazne and G. O'Connor, Nano-aluminum: Transport through sand columns and environmental effects on plants and soil communities, *Environ. Res.*, 2008, **106**, 296–303.
22 A. C. Bejarano, Critical review and analysis of aquatic toxicity data on oil spill dispersants, *Environ. Toxicol. Chem.*, 2018, **37**, 2989–3001.
23 L. Yang and D. J. Watts, Particle surface characteristics may play an important role in phytotoxicity of alumina nanoparticles, *Toxicol. Lett.*, 2005, **158**, 122–132.
24 G. V. Lowry, J. P. Giraldo, N. F. Steinmetz, A. Avellan, G. S. Demirer, K. D. Ristroph, G. J. Wang, C. O. Hendren, C. A. Alabi, A. Caparco, W. da Silva, I. González-Gamboa, K. D. Grieger, S.-J. Jeon, M. V. Khodakovskaya, H. Kohay, V. Kumar, R. Muthuramalingam, H. Poffenbarger, S. Santra, R. D. Tilton and J. C. White, Towards realizing nano-enabled precision delivery in plants, *Nat. Nanotechnol.*, 2024, **19**, 1255–1269.
25 C. Allará, G. Ciccone, M. Ciocca, S. Vasquez, P. Ibba, M. Maver, T. Mimmo, P. Lugli and L. Petti, Electronic Nanomaterials for Plants: A Review on Current Advances and Future Prospects, *Adv. Electron. Mater.*, 2025, 2500080.
26 D. Li, W. Li, H. Zhang, X. Zhang, J. Zhuang, Y. Liu, C. Hu and B. Lei, Far-Red Carbon Dots as Efficient Light-Harvesting Agents for Enhanced Photosynthesis, *ACS Appl. Mater. Interfaces*, 2020, **12**, 21009–21019.
27 H. Hu, W. Cheng, X. Wang, Y. Yang, X. Yu, J. Ding, Y. Lin, W. Zhao, Q. Zhao, R. Ledesma-Amaro, X. Chen, J. Liu, C. Yang and X. Gao, Enhancing Plant Photosynthesis using Carbon Dots as Light Converter and Photosensitizer, *bioRxiv*, 2024, DOI: **10.1101/2024.02.06.579025**.
28 T. Mandal, S. R. Mishra and V. Singh, Comprehensive advances in the synthesis, fluorescence mechanism and multifunctional applications of red-emitting carbon nanomaterials, *Nanoscale Adv.*, 2023, **5**, 5717–5765.
29 A. Dutta, R. R. Dutta and S. Gogoi, Optical properties of carbon dots and their applications, *Carbon Dots in Agricultural Systems: Strategies to Enhance Plant Productivity*, 2022, pp. 135–153.
30 M. S. Vezie, S. Few, I. Meager, G. Pieridou, B. Dörling, R. S. Ashraf, A. R. Goñi, H. Bronstein, I. McCulloch, S. C. Hayes, M. Campoy-Quiles and J. Nelson, Exploring the origin of high optical absorption in conjugated polymers, *Nat. Mater.*, 2016, **15**, 746–753.
31 M. Ciocca, P. Giannakou, P. Mariani, L. Cinà, A. Di Carlo, M. O. Tas, H. Asari, S. Marcozzi, A. Camaioni, M. Shkunov and T. M. Brown, Colour-sensitive conjugated polymer inkjet-printed pixelated artificial retina model studied via a bio-hybrid photovoltaic device, *Sci. Rep.*, 2020, **10**, 21457.
32 S. Vaquero, C. Bossio, S. Bellani, N. Martino, E. Zucchetti, G. Lanzani and M. R. Antognazza, Conjugated polymers for the optical control of the electrical activity of living cells, *J. Mater. Chem. B*, 2016, **4**, 5272–5283.
33 R. Kiebooms, R. Menon and K. Lee, Synthesis, electrical, and optical properties of conjugated polymers, *Handbook of Advanced Electronic and Photonic Materials and Devices*, 2001, pp. 1–102.
34 K. Namsheer and C. Sekhar Rout, Conducting polymers: a comprehensive review on recent advances in synthesis, properties and applications, *RSC Adv.*, 2021, **11**, 5659–5697.
35 K. M. Coakley and M. D. McGehee, Conjugated Polymer Photovoltaic Cells, *Chem. Mater.*, 2004, **16**, 4533–4542.
36 J.-T. Chen and C.-S. Hsu, Conjugated polymer nanostructures for organic solar cell applications, *Polym. Chem.*, 2011, **2**, 2707–2722.
37 E. Joseph, M. Ciocca, H. Wu, S. Marcozzi, M. A. Ucci, K. Keremane, L. Zheng, B. Poudel, C. Wu, A. Camaioni, K. Wang, S. Priya and T. M. Brown, Photovoltaic bioelectronics merging biology with new generation semiconductors and light in biophotovoltaics photobiomodulation and biosensing, *npj Biosens.*, 2024, **1**, 15.
38 C. Allarà, A. Orlando, G. Ciccone, S. Krik, M. Pompilio, A. Pedrielli, A. Gaiardo, P. Lugli, L. Petti, F. Cacialli and M. Ciocca, Conjugated Polymer Nanoparticles for Biophotonic Applications: Preparation, Characterization, and Simulation in Biohybrid Interfaces, *Adv. Electron. Mater.*, 2025, 2500073.
39 M. Ciocca, S. Marcozzi, P. Mariani, V. Lacconi, A. Di Carlo, L. Cinà, M. D. Rosato-Siri, A. Zanon, G. Cattelan, E. Avancini, P. Lugli, S. Priya, A. Camaioni and T. M. Brown, A Polymer Bio–Photoelectrolytic Platform for Electrical Signal Measurement and for Light Modulation of Ion Fluxes and Proliferation in a Neuroblastoma Cell Line, *Adv. Nanobiomed. Res.*, 2023, **3**, 2200127.
40 E. Zucchetti, M. Zangoli, I. Bargigia, C. Bossio, F. Di Maria, G. Barbarella, C. D'Andrea, G. Lanzani and M. R. Antognazza, Poly(3-hexylthiophene) nanoparticles for biophotonics: study of the mutual interaction with living cells, *J. Mater. Chem. B*, 2017, **5**, 565–574.
41 Y. Wang, S. Li, L. Liu, F. Lv and S. Wang, Conjugated Polymer Nanoparticles to Augment Photosynthesis of Chloroplasts, *Angew. Chem., Int. Ed.*, 2017, **56**, 5308–5311.
42 L. M. Cavinato, E. Fresta, S. Ferrara and R. D. Costa, Merging Biology and Photovoltaics: How Nature Helps Sun-Catching, *Adv. Energy Mater.*, 2021, **11**, 2100520.

43 X. Zhou, Y. Zeng, F. Lv, H. Bai and S. Wang, Organic Semiconductor–Organism Interfaces for Augmenting Natural and Artificial Photosynthesis, *Acc. Chem. Res.*, 2022, **55**, 156–170.
44 V. K. Oikonomou, M. Huerta, A. Sandéhn, T. Dreier, Y. Daguerre, H. Lim, M. Berggren, E. Pavlopoulou, T. Näsholm, M. Bech and E. Stavrinidou, eSoil: A low-power bioelectronic growth scaffold that enhances crop seedling growth, *Proc. Natl. Acad. Sci. U. S. A.*, 2024, **121**(2), e2304135120.
45 L. Kutzbach, J. Schneider, T. Sachs, M. Giebels, H. Nykänen, N. J. Shurpali, P. J. Martikainen, J. Alm and M. Wilmking, CO2 flux determination by closed-chamber methods can be seriously biased by inappropriate application of linear regression, *Biogeosciences*, 2007, **4**, 1005–1025.
46 P. Zhao, A. Hammerle, M. Zeeman and G. Wohlfahrt, On the calculation of daytime CO2 fluxes measured by automated closed transparent chambers, *Agric. For. Meteorol.*, 2018, **263**, 267–275.
47 S. H. van Delden, M. J. Nazarideljou and L. F. M. Marcelis, Nutrient solutions for Arabidopsis thaliana: a study on nutrient solution composition in hydroponics systems, *Plant Methods*, 2020, **16**, 72.
48 P. Ballikaya, I. Brunner, C. Cocozza, D. Grolimund, R. Kaegi, M. E. Murazzi, M. Schaub, L. C. Schönbeck, B. Sinnet and P. Cherubini, First evidence of nanoparticle uptake through leaves and roots in beech (Fagus sylvatica L.) and pine (Pinus sylvestris L.), *Tree Physiol.*, 2023, **43**, 262–276.
49 F. Di Maria, A. Zanelli, A. Liscio, A. Kovtun, E. Salatelli, R. Mazzaro, V. Morandi, G. Bergamini, A. Shaffer and S. Rozen, Poly(3-hexylthiophene) Nanoparticles Containing Thiophene- *S*, *S* -dioxide: Tuning of Dimensions, Optical and Redox Properties, and Charge Separation under Illumination, *ACS Nano*, 2017, **11**, 1991–1999.
50 Y. Su, V. Ashworth, C. Kim, A. S. Adeleye, P. Rolshausen, C. Roper, J. White and D. Jassby, Delivery, uptake, fate, and transport of engineered nanoparticles in plants: a critical review and data analysis, *Environ. Sci.: Nano*, 2019, **6**, 2311–2331.
51 S. Park, J. Jeong, G. Hyun, M. Kim, H. Lee and Y. Yi, The origin of high PCE in PTB7 based photovoltaics: proper charge neutrality level and free energy of charge separation at PTB7/PC71BM interface, *Sci. Rep.*, 2016, **6**, 35262.
52 H. Hintz, H.-J. Egelhaaf, H. Peisert and T. Chassé, Photooxidation and ozonization of poly(3-hexylthiophene) thin films as studied by UV/VIS and photoelectron spectroscopy, *Polym. Degrad. Stab.*, 2010, **95**, 818–825.
53 R. Wei, M. Gryszel, L. Migliaccio and E. D. Głowacki, Tuning photoelectrochemical performance of poly(3-hexylthiophene) electrodes *via* surface structuring, *J. Mater. Chem. C*, 2020, **8**, 10897–10906.
54 G. Avola, A. Matese and E. Riggi, An Overview of the Special Issue on "Precision Agriculture Using Hyperspectral Images, *Remote Sens.*, 2023, **15**, 1917.
55 R. Lei, H. Jiang, F. Hu, J. Yan and S. Zhu, Chlorophyll fluorescence lifetime imaging provides new insight into the chlorosis induced by plant virus infection, *Plant Cell Rep.*, 2017, **36**, 327–341.
56 J.-D. Rochaix, Regulation of photosynthetic electron transport, *Biochim. Biophys. Acta, Bioenerg.*, 2011, **1807**, 375–383.
57 N. Nelson and A. Ben-Shem, The structure of photosystem I and evolution of photosynthesis, *BioEssays*, 2005, **27**, 914–922.
58 A. V. Ruban, M. P. Johnson and C. D. P. Duffy, Natural light harvesting: principles and environmental trends, *Energy Environ. Sci.*, 2011, **4**, 1643.
59 T. Mirkovic, E. E. Ostroumov, J. M. Anna, R. van Grondelle, R. Govindjee and G. D. Scholes, Light Absorption and Energy Transfer in the Antenna Complexes of Photosynthetic Organisms, *Chem. Rev.*, 2017, **117**(2), 249–293.
60 H. Mondal, S. K. Ray, P. Chakrabarty, S. Pal, G. Gangopadhyay, S. Das, S. Das and R. Basori, High-Performance Chlorophyll-b/Si Nanowire Heterostructure for Self-Biasing Bioinorganic Hybrid Photodetectors, *ACS Appl. Nano Mater.*, 2021, **4**, 5726–5736.

